Predicting *Escherichia coli's* Chemotactic Drift under Exponential Gradient

Sibendu Samanta,[1] Ritwik Layek,[1,*] Shantimoy Kar,[2] Kiran Raj M,[2] Sudipta Mukhopadhyay,[1] and Suman Chakraborty[2, 3, 4,*]

[1]*Department of Electronics and Electrical Communication Engineering*
[2]*Advanced Technology Development Centre*
[3]*Microfluidic Laboratory, Department of Mechanical Engineering*
[4]*School of Medical Science and Technology,*
Indian Institute of Technology, Kharagpur, WB-721302, India

Abstract: Bacterial species are known to show chemotaxis, i.e. the directed motions in presence of certain chemicals, whereas the motion is random in absence of those chemicals. The bacteria modulate their run-time to induce chemotactic drift towards the attractant chemicals and away from the repellent chemicals. However, the existing theoretical knowledge doesn't exhibit proper match with experimental validation and hence there is a need of developing alternate models and validate experimentally. In this manuscript a more robust theoretical model is proposed to investigate chemotactic drift of peritrichous *Escherichia coli* under an exponential nutrient gradient. Exponential gradient is used to understand the steady state behavior of drift because of the logarithmic functionality of the chemosensory receptors. Our theoretical estimations are validated through the experimentation and simulation results. Thus, the developed model successfully delineates the run-time, run trajectory, and drift velocity as measured from the experiments.

Email: suman@mech.iitkgp.ernet.in and ritwik@ece.iitkgp.ernet.in

I. INTRODUCTION

Bacteria, one of the abundant microorganisms, utilize different mechanisms for their survival as well as growth. Understanding these particular mechanisms is very crucial to perceive the bacterial motility at different environmental conditions. Most of the bacterial species are known to respond through different external perturbations like air, magnetic field, light, and predominantly chemicals. For majority of the scenarios, chemotactic movement of bacterium has been exploited to comprehend the internal feedback mechanism of the species [1]. In the literature, both experimental and numerical techniques have been adopted to explain the underlying trends, with some degree of success [2–4]. To quantify the bacterial motility, drift velocity has been considered as the most useful parameter. Till date, one of the key challenges lies in developing a successful model to predict the chemotactic drift of bacteria [5]. Apart from the obvious necessity of modeling any physical or chemical process, there is another piece of historic perspective to motivate our research in drift. In the early twentieth century, electricity was discovered as drift of electrons in a conducting bar subject to an external electric field. The theory of diffusion of electron in a conducting bar without the electric field arises from thermodynamic considerations. Understanding drift of electron opens up a new domain of expertise in electrical transport and electronics. Similarly to understand biological transport in different organisms, it is important to develop computationally tractable and reliable predictive model of drift in biology. In this particular work, our entire study is focused to predict the chemotactic motility of *E. coli* for theoretical and experimental understanding.

Bacterial motility can be understood from the chemo-sensory circuit of the bacteria. Fig. 1 represents a detailed mechanism of the bacterial sensing. The chemotaxis pathway of *E. coli* is equipped with a chemo-sensing receptor cluster to sense the chemical environment [6–8], logarithmic sensing capability to incorporate the dynamic range of reception [9–11], an integral feedback mechanism to incorporate adaptation with the changing external chemical environment [12], signal transduction pathways to carry the sensory information to the flagellar motor in real time [13], the coupling mechanism to switch between flagellar bundle formations [14,15], and rotational diffusion [16].

E. coli senses the ligand concentration from its surroundings to govern the rotation of flagellar motor [17–19]. During default counter-clockwise (CCW) rotation (looking from the flagella to bacteria) of the motor, all the flagella bundle together and generate a repulsive force which drives the bacteria forward (i.e. run). Whenever one or more motors start rotating in the clockwise (CW) direction, the flagellum comes out of the bundle, thus bacterium changes its direction (i.e. tumble). Phosphorylated form of CheY messenger (phospho-CheY) binds with the motors and increases the tumbling rate i.e. the switching rate from CCW to CW. Periplasmic domain of a methyl-accepting protein (MCP) binds with the ligand molecules which modulates the auto-phosphorylation activity of histidine kinase CheA (and CheW as well) through its cytoplasmic domain. Due to ligand binding, auto-phosphorylation activity of CheA decreases. Receptor's activity always adapts itself through a negative integral feedback mechanism to sense the differential alteration in the ligand concentration.

Receptor's activity depends on the methylation level, and the rate of methylation is controlled by a fine balance between two proteins, namely methyltransferase (CheR) and methylesterase (CheB). The phosphatase activities are controlled by CheZ which dephosphorylates phospho-CheY to CheY [20–23].

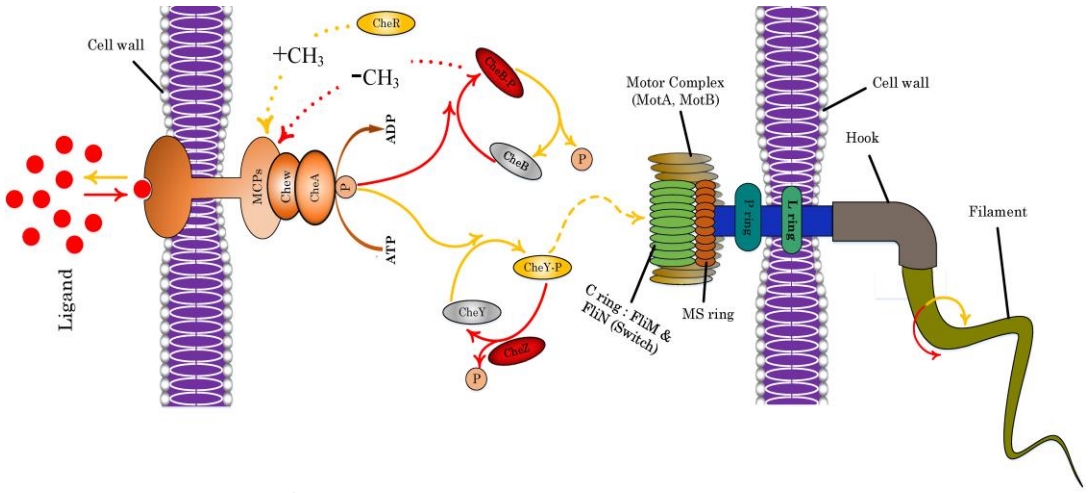

FIG. 1. Schematic details of the bacterial chemo-sensory network [31,32]. Gold color (lines, dashed lines, dotted lines, and shaded areas): elements and reactions that tag on CW flagellar rotation; red color (lines, dotted lines, and shaded areas): CCW-enhancing components. The response of regulatory proteins (CheB and CheY) are inactive (gray) until phosphorylated.

In this manuscript, we primarily focus on developing a theoretical construct to understand the unicellular motility of bacteria. To comprehend the logarithmic sensing of *E. coli*, an exponential ligand concentration profile is considered and thereafter the same is validated using an exponential ligand concentration profile in a microfluidic environment. Our theoretical consideration successfully predicts the run-time modulation and drift dynamics, which is further validated from the experimental settings.

II. THEORETICAL MODELING

We categorize the theoretical construct in three different sections: (A) Chemotaxis Network Dynamics, (B) Run-time Modulation, and (C) Drift Velocity.

A. Chemotaxis Network Dynamics

In Fig. 2, the ligand concentration L at any arbitrary location (x, y) is given by $L(x,y) = L_o e^{rx}$, where L_o and r are ligand concentration at $x = 0$ and exponential *ramp* constant respectively. The bacterium starts its $(k+1)^{th}$ run at a time t_k from location (x_k, y_k). It is indeed essential to transform the spatial ligand concentration profile to a temporal one, as the bacterium is known to sense the spatial gradient in a temporal way [24]. The

instantaneous velocity (v) is assumed to be constant during the run [25]. If the angle between $(k+1)^{th}$ run trajectory and the x axis is θ_k, the x-coordinate at time t during this run is given by

$$x(t) = x_k + v(\cos\theta_k)(t - t_k) = x_k + v(\cos\theta_k)\tau \tag{1}$$

where, $\tau = t - t_k$ is run-time. The ligand concentrations at (x_k, y_k) and $(x(t), y(t))$ are given as follows:

$$\begin{aligned} L_k &= L(x_k, y_k) = L_o e^{rx_k} \\ L(t) &= L(x(t), y(t)) = L_k e^{rv(\cos\theta_k)(t-t_k)} = L_k e^{rv(\cos\theta_k)\tau} \end{aligned} \tag{2}$$

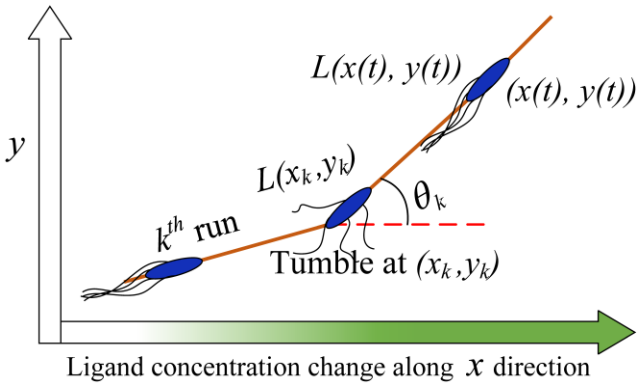

FIG. 2. Schematic representation of the bacterial run. In absence of chemical gradient, average run and tumble time are typically 1s and 0.1s respectively. Biased random movement of *E. coli* exhibits in presence of chemical gradient ($L(x,y)$). Temporal comparisons of chemo-attractant concentrations are made during run [24] with constant instantaneous velocity (v~*20*μm/s). Run-time is modulated based on gradient of chemo-attractant, before the chemotactic response is reset by methylation adaptation.

Receptor-complex activity is modeled as a single variable $a(t)$, where $a(t) = 0$ implies no phosphorylation activity of CheW-CheA kinase is taking place. Hence, CheY does not phosphorylate which results in a default perpetual CCW rotation of the flagellar motor. At another extreme, $a(t) = 1$ corresponds to the maximal activity of CheW-CheA kinases, resulting in saturation of tumbling frequency. Methylation level of the receptor is defined as $m(t)$. Considering above parameters, the dynamics of chemotaxis [26] can be represented as follows:

$$a(t) = \frac{1}{1 + e^{N\left[\ln\left(\frac{1+\frac{L(t)}{K_{ia}}}{1+\frac{L(t)}{K_a}}\right) + \alpha(m_o - m(t))\right]}} \approx \frac{1}{1 + e^{N\left[\ln\left(\frac{L(t)}{K_{ia}}\right) + \alpha(m_o - m(t))\right]}} = \frac{1}{1 + e^{\left[u(t) + \alpha N(m_o - m(t))\right]}} \tag{3}$$

$$\frac{dm(t)}{dt} = F(a(t)) \tag{4}$$

where m_o is initial methylation level of the receptor complex, α is the scaling of the methylation level, N defines the number of ligand-binding units in every receptor, and K_a and K_{ia} are the dissociation constants for the active and inactive receptors, respectively. For Eq. 3, it is assumed that $K_{ia} << L(t) << K_a$. The block diagram in Fig. 3 schematically represents details of the theoretical consideration.

The pre-filtered signal $u(t)$ can be computed for the spatial exponential ligand field and is presented in Eq. 5.

$$u(t) = N\,ln\left[\frac{L(t)}{K_{ia}}\right] = N\,ln\left[\frac{L_k}{K_{ia}}e^{rv(\cos\theta_k)\tau}\right] = N\,ln\left[\frac{L_k}{K_{ia}}\right] + Nrv(\cos\theta_k)\tau = u_k + \sigma_k\tau \tag{5}$$

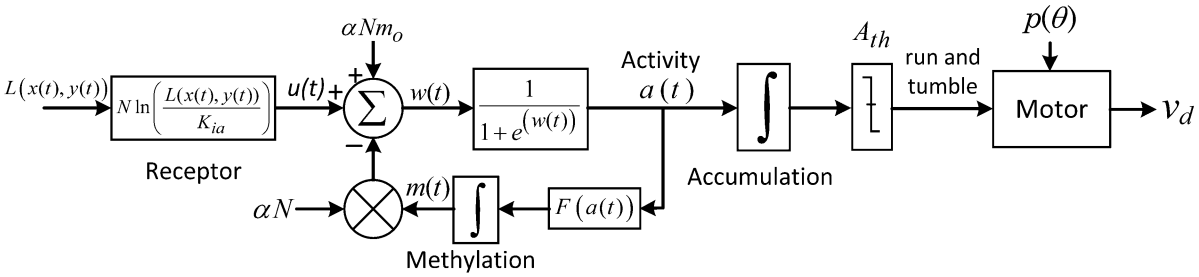

FIG. 3. Block diagram of the chemotaxis network for $K_{ia} << L(x(t),y(t)) << K_a$. Here, $w(t) = u(t) + \alpha N(m_o - m(t))$.

where, σ_k and u_k are updated at every tumble. Methylation rate $\frac{dm}{dt}$ is a monotonically decreasing function over the range of $a(t)$. $F(0) = K_R$ i.e. maximum methylation rate by methyltransferase CheR and $F(1) = K_B$ is the maximum demethylation rate by methylesterase CheB. Several possibilities can be chosen for the function $F(a(t))$, but the linear one is the most intuitive and meaningful. However, it is possible to experimentally estimate $F(a(t))$. In this manuscript, Eq. 6 is used as a choice of methylation rate [27].

$$F(a(t)) = K_R - (K_R + K_B)a(t) \tag{6}$$

The receptor-complex activity $a(t)$ can be expressed as follows:

$$a(t) = \frac{1}{1+e^{\left[(u_k+\sigma_k\tau)+\alpha N(m_o-m(t))\right]}} = \frac{1}{1+\xi_k e^{\sigma_k t - \alpha N m(t)}} \tag{7}$$

where, $\xi_k = e^{u_k - \sigma_k t_k + \alpha N m_o}$. The rate of change of receptor-complex activity can be expressed as follows:

$$\frac{da(t)}{dt} = a(t)(1-a(t))[\alpha NF(a(t)) - \sigma_k] \tag{8}$$

So, run-time τ can be obtained from the following expression:

$$\begin{aligned} \tau &= \int_{t_k}^{t} dt = \int_{a_o^k}^{a(t)} \frac{da}{a(t)(1-a(t))[\alpha NF(a(t)) - \sigma_k]} \\ &= ln\left[\frac{a(t)^{A_k}}{(1-a(t))^{B_k}(\beta_k - a(t))^{C_k}}\right] - \gamma_k = G_k(a(t)) - \gamma_k \end{aligned} \tag{9}$$

where, $\gamma_k = G_k(a_o^k)$, $A_k = \frac{\xi}{\beta_k}$, $B_k = \frac{\xi}{\beta_k - 1}$, $C_k = \frac{-\xi}{\beta_k(\beta_k - 1)}$, $\xi = \frac{1}{\alpha N(K_R + K_B)}$, and $\beta_k = \frac{\alpha N K_R - \sigma_k}{\alpha N(K_R + K_B)}$. The analytical expression of the state of the system is thus given by

$$a(t) = G_k^{-1}(\tau + \gamma_k) = G_k^{-1}(t - t_k + \gamma_k) \tag{10}$$

For this particular dynamical systems, there are two unstable points at $a(t) = 0$ and $a(t) = 1$, and one stable fixed point at $a(t) = \beta_k$. For every run, receptor activity $a(t)$ moves towards the stable fixed point β_k, and thus at every tumble β_k value is updated.

B. Run-time Modulation

Another important aspect of bacterial chemotactic drift is run-time modulation. Considering the fundamentals of tumbling phenomena, theoretical understanding of run-time modulation can be developed. Phospho-CheY molecules transport through cytoplasm and bind with the rotor. Whenever the accumulation of phospho-CheY crosses a threshold value, the rotor switches its direction to CW, which in effect unfolds the flagellar bundle. Rotational diffusion decides the new direction during the tumble, therefore the rotor resets to its default CCW direction to start its next run. Since phosphorylation of CheY is directly controlled by the complex-receptor activity $a(t)$, an empirical threshold A_{th} can be constructed such that when $\int_0^{\tau} a(t)dt$ crosses the threshold A_{th}, tumble takes place, providing a run-time of τ. Hence the run-time in the $(k+1)^{th}$ run can be defined as

$$\tau_k(r) = \tau(a_o^k, \theta_k, r) = \arg\min_{\tau}\left[\left|\int_0^{\tau} a(a_o^k, \theta_k, r, t)dt - A_{th}\right|\right] \tag{11}$$

where $a_o^k = a(t_k)$ is the initial state of the $(k+1)^{th}$ run and θ_k is the angle of the $(k+1)^{th}$ run trajectory with the positive *x*-axis. This construction is in accordance with the prior experimental evidence. In the absence of any ligand concentration gradient, if the average run-time is τ^* and the receptor activity is a^* ($\tau^* = 1s, a^* = 0.33$ in [26]), A_{th} can be computed as Eq. 12.

$$A_{th} = \int_0^{\tau^*} a^* \, dt = a^* \tau^* \tag{12}$$

Consider a temporal exponentially increasing attractant ramp $L(t) = L_o e^{rt}$, where $r < r_{sat}$ (as described in [26]). From the literature, it is known that $a(t)$ will attain a steady state $a_r < a^*$. So the tumbling frequency will decrease from its original value ($f^* = 1/\tau^*$), because, $f_r = \frac{1}{\tau_r} = (\frac{a_r}{A_{th}}) < (\frac{a^*}{A_{th}}) = f^*$. Similarly, for exponentially decreasing attractant gradient or exponentially increasing repellent gradient, the tumbling frequency increases. $\tau(a_o^k, \theta_k, r)$ is the modulated run-time (Eq. 11). Tumble angle follows a probability density function $p(\theta)$ [20,25] which is assumed to be identical for different r, θ_k, and a_o^k. The empirical expression of $p(\theta)$ is shown in Eq. 13 [27] and in Fig. S1 of the *Supplemental Material* [33]. The current trajectory angle θ_k with the positive x-axis is essentially the cumulative sum of all k tumble angles and the angle of the initial run with the positive x-axis.

$$p(\theta) = \begin{cases} -0.25(1+\cos\theta)\sin\theta & \forall \theta \in (-\pi, 0] \\ 0.25(1+\cos\theta)\sin\theta & \forall \theta \in (0, \pi] \end{cases} \tag{13}$$

C. Drift Velocity

The block diagram of chemotaxis module is shown in Fig. 3. The prior history at the beginning of $(k+1)^{th}$ run is stored in the parameters $a_o^k \in [0,1]$ and $\theta_k \in (-\pi, \pi]$. $\theta_k = \theta_{k-1} + \theta$, where $\theta \sim p(\theta)$ (from Eq. 13). Although a_o^k is not an explicit random variable, a_o^k depends on the run-time of k^{th} run (τ_{k-1}) and the trajectory angle of k^{th} run with the positive x-axis (θ_{k-1}). Hence, this implicit stochasticity in a_o^k along with the stochasticity of θ_k denies the direct construction of drift velocity from the otherwise deterministic chemotaxis dynamics. By definition, drift velocity is thus expected to be computed over these two random variables. Assume $p_r(a_o)$ to be the probability density function (pdf) of a_o^k for successive run-tumbles. Hence, for given one-dimensional ligand field $L(x,y) = L_o e^{rx}$, the chemotactic drift velocity can be

$$v_d(r) = \frac{\underset{a_o}{E}\left[\underset{\theta}{E}\{v(\cos\theta)\tau(a_o,\theta,r)\}\right]}{\underset{a_o}{E}\left[\underset{\theta}{E}\{\tau(a_o,\theta,r)\}\right]} = v\frac{\int_{a_o}\int_{\theta} \tau(a_o,\theta,r)(\cos\theta)\, p_r(a_o)\, p(\theta) d\theta da_o}{\int_{a_o}\int_{\theta} \tau(a_o,\theta,r)\, p_r(a_o)\, p(\theta) d\theta da_o} \tag{14}$$

$p_r(a_o)$ is required to be computed (for algorithm see Algorithm 1 in *Supplemental Material* [33]) from the chemotaxis dynamics by successive runs. For different values of r, the probability density functions are estimated by computer simulation and are shown in Fig. 4. For instance, at $r = 0$, the state variable $a_o = a^*$ is a fixed point. Hence, $p_{r=0}(a_o)$ is a Dirac

delta function at $a_o = a^*$. As r increases, the distributions spread out. The empirical $p(\theta)$ and the simulated $p_r(a_o)$ are used for the Monte-Carlo computation of drift velocity (i.e. Eq. 14).

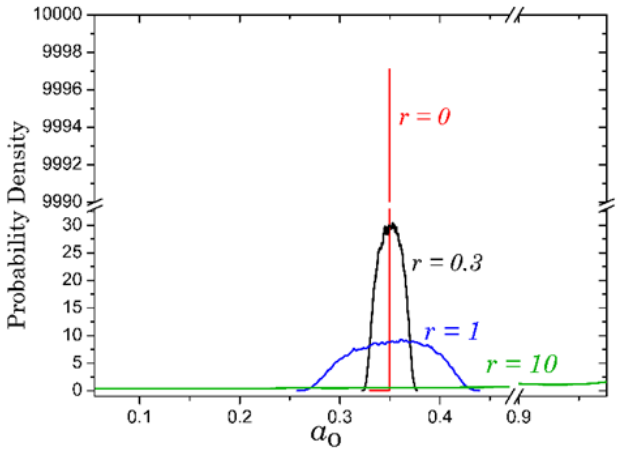

FIG. 4. Probability density of the initial condition of state (a_o) for different values of r. 10^6 runs of 10^5 bacteria for every r is simulated for estimating probability density.

III. EXPERIMENTAL DETAILS

Jiang et. al [17] developed the theoretical basis for chemotactic drift velocity and validated indirectly using FRET microscopy based experiments. However, the experiments were not on bacterial dynamics and motion trajectory. Similarly, Reneaux et. al [28] designed the drift velocity for weak gradient and subsequently presented a comparative study with the exiting literature results [5] (T. Ahmed and R. Stocker) to validate their model. T. Ahmed and R. Stocker [5] illustrated a microfluidic approach where the nutrient changes exponentially with time, which is believed as an appropriate approach to investigate the adaptation mechanism of the chemotactic network. Considering the three dimensional alteration of the ligand field in real systems, we believe that it is essential to consider the spatio-temporal variation of ligand field. So, a 'premixing-micro-channel' (shown in Fig. 5) having a dimension of $l = 20\,mm$, $h = 25\mu m$, $w = 975\mu m$, and $p = 4.3mm$ was designed to develop the spatial gradient of the nutrient for our microfluidic experiment. Channel dimensions ensure the free movement of bacteria through the micro-conduit. Photo-lithography and subsequently soft lithography were followed to fabricate the micro-channel and thereafter bonded using oxygen-plasma bonding chamber.

Through two inlets of the 'premixing-micro-channel', bacterial suspension [*E. coli, DH5α* (2×10^5 cfu/ml) suspended in phosphate buffer saline (PBS) of pH ~ 7.4] and dextrose solution ([0, 10] mM) were transported using syringe pump at a flow rate of $0.05\mu l$ / min . Bright field phase contrast microscopy (OLYMPUS IX71, 40X objective lens) was used to capture the bacterial transport and thereafter post-processed using MATLAB. To study the bacterial movement, measurements were performed in stopped flow conditions i.e. after *10*s of the

initialization period which minimizes the inertial effect. Generation of ligand concentration gradient is evident from Fig. 6 (for details please refer to Section S1 of *Supplemental Material* [33]).

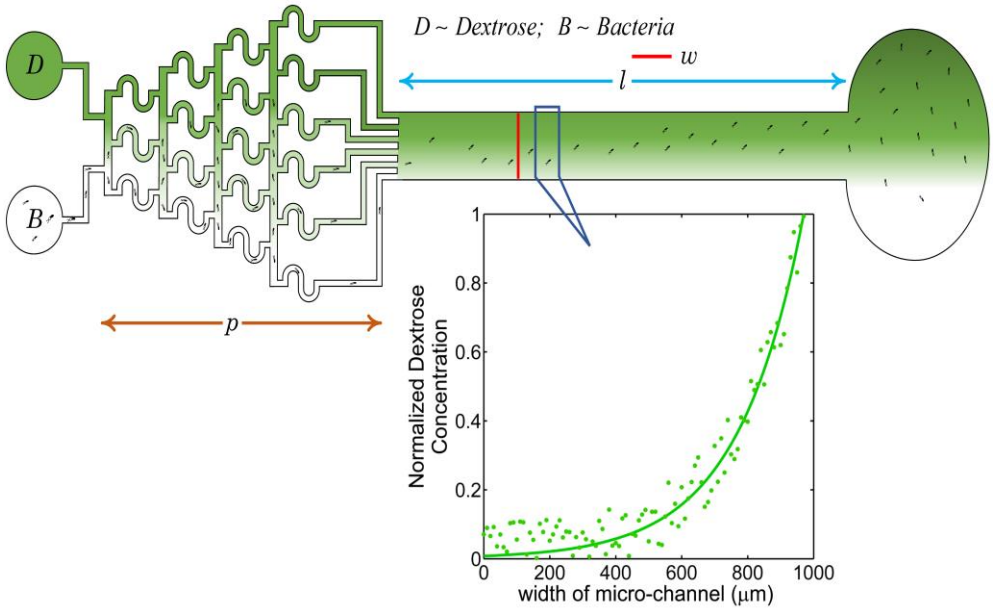

FIG. 5. Schematic of the premixing-micro-channel in which 'D' and 'B' reservoirs represent the inlets of dextrose and bacterial solution, respectively. Inset figure shows that an exponential ligand concentration profile is generated along the width of the micro-channel. An image of the experimental settings is shown in Fig. S3 of the *Supplemental Material* [33].

IV. RESULTS and DISCUSSIONS

A. Estimation of Bacterial Trajectories

Tumbling position (x_k, y_k) is ascertained from the bacterium's trajectory at t_k, while the tumbling angle (θ_k) made by the instantaneous velocity of the bacterium with positive *x*-axis at t_k is given by $\theta_k = \lim_{\Delta x_k \to 0} tan^{-1}\left(\frac{\Delta y_k}{\Delta x_k}\right) = tan^{-1}\left(\frac{y_{k+1} - y_k}{x_{k+1} - x_k}\right)$. The angle at every tumbling position for experimental and simulated trajectories is exhibited in Fig. 7. From Fig. 7, it is evident that increasing *'r'* values lead to the increment in run-time.

For the spatial exponential ligand field $L(x,y) = L_o e^{rx}$, run-time, $\tau(a_o^k, \theta_k, r)$, can be plotted as a function of θ_k for a choice of a_o and r using Eq. 11. Experimental run-time modulation with respect to θ_k is observed for different concentrations of dextrose solutions. The theoretical and experimental run-time contours for different r values (for $a_o = a^*$) are shown in Fig. 8. From the figure, it is clearly evident that for $r=0$ i.e. in absence of dextrose solution, run-time is measured to be *1*s. When the dextrose concentration is increased to $r=5$, run-time is measured

to ~ *1.27* s; whereas for *r=8*, run-time is seen to be ~ *1.7* s (for $\theta_k = 30^o$). These contours graphically represent the differential biases at different *r* and explain the chemotactic drift along the negative gradients of dextrose solution (i.e. opposite direction of the increasing dextrose concentration).

B. Estimation of Drift Velocity

Usually, drift velocity is defined as the ensemble average velocity [25,29,30]. In a spatial ligand field, the trajectory is not sufficient enough to capture the alterations in drift velocity. Therefore, an algorithm is designed to estimate the drift velocity from the trajectory of a single bacterium (or a handful of bacteria). It is assumed that all bacteria start from the origin of the two-dimensional space and have identical a_o^o.

The tumble coordinates and the run-times can easily be obtained from the trajectory data. From the run-time contours that are shown in Fig. 8 and in Fig. S2 *of Supplemental Material* [33], it is evident that every run has two components: one is due to the average random movement, which can be defined as 'diffusion' process, and the second is the biased movement which is the desired 'drift'. Hence, the drift should be measured in a particular trajectory at those points where the cumulative diffusion component of the motion crosses the baseline (here, the *x*-axis). The algorithm for estimating v_d from trajectories is shown in Algorithm 3 *of Supplemental Material* [33].

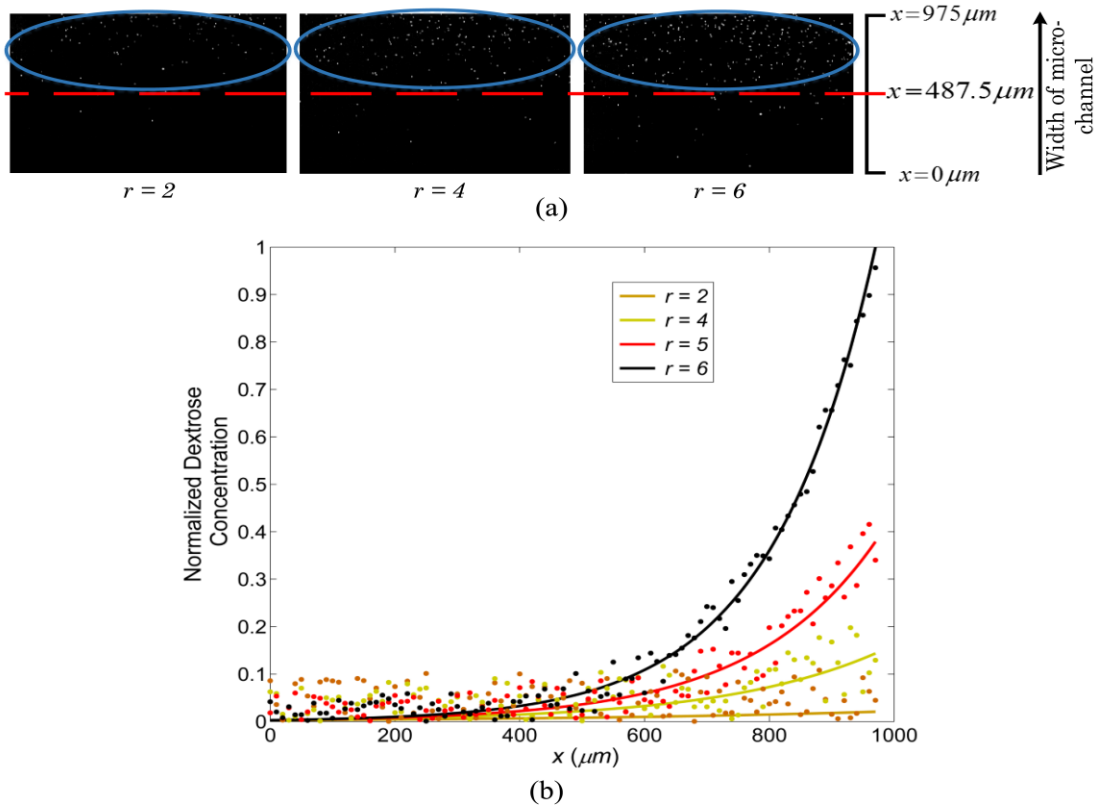

FIG. 6. Exponential ligand concentration in the premixing-micro-channel. (a) micro-beads concentration in premixing-micro-channel for different value of ramp *r*. The marked region (i.e. oval-shaped region) shows increasing concentration of beads; and (b) Ligand (dextrose) concentration in the premixing-micro-channel: The spatio-localization of the dextrose molecules are given by dots and the least square fitted curves are also shown to represent the smooth spatial exponential ramp ligand concentration $L(x,y)=L_o e^{rx}$ for different value of ramp (r).

The dynamic range of bacterial sensors is $10^6 \cong e^{14}$ i.e., r values lies in [0, 14]. Thus, we use $0 \le r \le 10$ in our experiments and simulations. Fig. 9 delineates the fact that increase in r values leads to the enhancement of chemotactic drift, however drift velocity reaches to a plateau for $r=7$ or more. Our theoretical results resemble with the experimental as well as simulated results; thus provide a direct validation of the proposed modeling scheme. Furthermore, the resemblance of the drift velocity from untethered *E. coli*'s trajectory in the microfluidic channel and the simulated trajectory with the theoretically derived results provide a proof to the concept of the estimation algorithm.

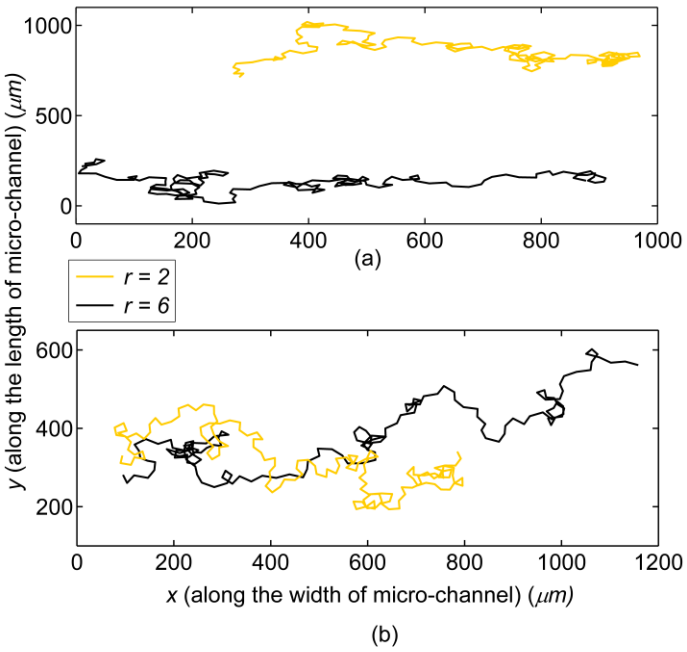

FIG. 7. Bacterial trajectory for different values of *r*. (a) Experimental ((b) simulated) trajectories with time-lapse of 233s (235s) and 152s (137s) are considered for *r = 2* and *r = 6*, respectively. Algorithm 2 in *Supplemental Material* [33] is followed to generate simulated bacterial trajectory.

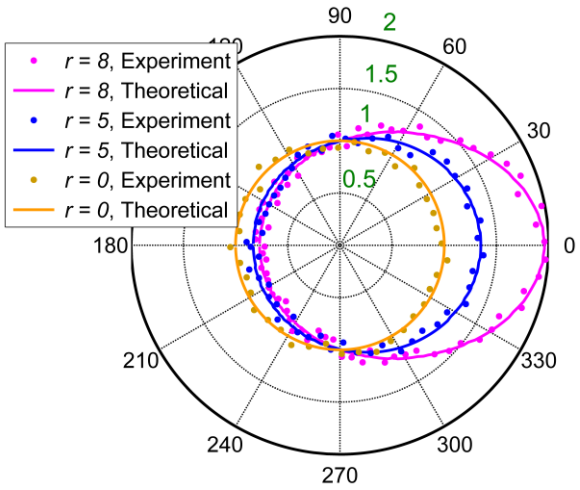

FIG. 8. Theoretical and experimental run-time contours with respect to θ_k for different values of *r* ($a_o = a^*$). Here, mean of experimental run-times are presented in this contour at every θ_k for particular value of *r*. Untethered *E. coli* movement is observed in microfluidic chemical gradient by microscope. Tumbling angle and position are measured from untethered bacterial trajectory using image processing. The run-time $\tau(a_o^k,\theta_k,r)=\frac{v}{\sqrt{(x_{k+1}-x_k)^2+(y_{k+1}-y_k)^2}}$ is calculated from trajectory and the polar plot of run-time is drawn for particular value of *r*. The theoretically derived run-time contour with respect to θ_k for different value of a_o (for constant *r*) is shown in Fig. S2 *of the Supplemental Material* [33].

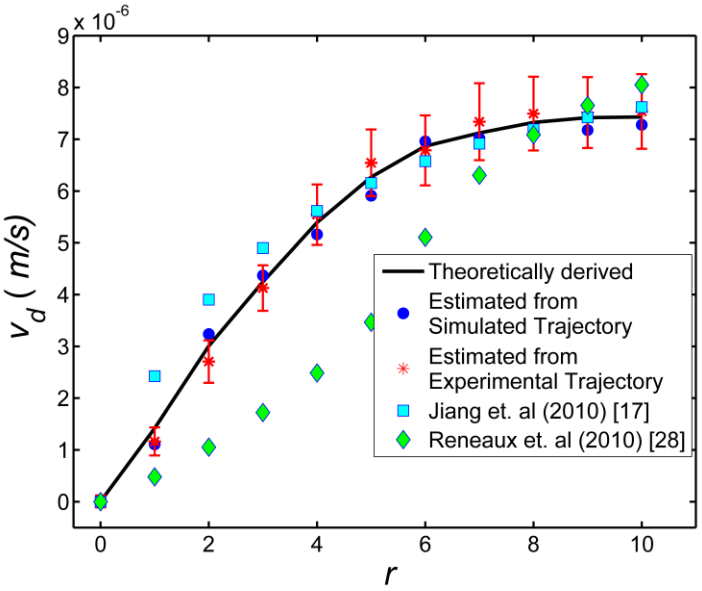

FIG. 9. Drift velocity (v_d) for different values of r. The theoretical and simulated estimate v_d are compared with experimental estimated v_d. Error bars of the graph are defined by $\mu \pm \sigma$. Where, μ and σ are the mean and the standard deviation of drift velocities as collected from the repeated sets of experiments. For this analysis, 57 experimental observations and 500 simulation observations are considered for every r. For simulation, only the mean results (•) are displayed. The results are also compared with two empirical models, Jiang et. al [17] and Reneaux et. al [28] (for details please refer to Section S2 of *Supplemental Material* [33]).

IV. Conclusions

In this manuscript, a new theoretical model of the chemotactic drift has been developed. The model is studied for steady state drift velocity under spatial exponential nutrient gradients. The trajectory simulation based on this model is considered for testing the drift velocity estimation algorithm. The microfluidics based experiments are carefully designed to validate both the proposed model as well as the trajectory based estimation process. The most important aspect of this work is validation of chemotaxis using untethered bacteria trajectory in microfluidic channels. Changing the channel topology, several other spatial and spatio-temporal profiles can be generated to study the nonlinear chemotaxis network. Setting the initial nutrient profile as a step function in a Y-channel and then allowing the step function to diffuse, provides an environment to study the chemotactic step response. Similarly frequency response of the system can be studied by creating exponential sinusoidal nutrient gradients in specially designed channel. These different experiments unravel the dynamics of the chemotaxis network in a better way. We believe that this work will be helpful to the researchers to design intervention strategies for controlling the chemotactic drift, which can be further extended to control of population dynamics of *E. coli*. Possible shortcomings of this kind of study include the input-output chemotaxis model validation. Here changing the input nutrient profile the output drift velocity is studied to understand the underlying network dynamics. Using this methodology it will not be possible to answer specific questions regarding gene-protein regulations in the chemotaxis circuitry. Introducing genetic tags (e.g.,

green fluorescent protein) for studying such genes and proteins in the moving bacteria and then estimating the active proteins' concentration from the fluorescence can help in removing such shortcomings.

Acknowledgement

Authors would like to thank the Micro-Electronics Laboratory, Dept. of E and ECE, IIT Kharagpur for providing the mask fabrication facilities. S.K would like to thank Royal Academy of Engineering, UK for his research fellowship. S.S. and S.K. would like to specially thank Mr. Joyjyoti Das (Reseach Scholar, Biotechnology, IIT Kharagpur) for his initial assistance in developing the experimental setup and it's optimization. The work was partly supported by the project WBC funded by Indian Institute of Technology, Kharagpur.

References:

[1] J. Adler, Science (80-.). **153**, 708 (1966).

[2] H. C. Berg, Annu. Rev. Biophys. Bioeng. **4**, 119 (1975).

[3] J. S. Parkinson, Cell **4**, 183 (1975).

[4] H. C. Berg, *E. Coli in Motion* (Springer Science & Business Media, 2008).

[5] T. Ahmed and R. Stocker, Biophys. J. **95**, 4481 (2008).

[6] H. C. Berg and E. M. Purcell, Biophys. J. **20**, 193 (1977).

[7] A. Vaknin and H. C. Berg, J. Mol. Biol. **366**, 1416 (2007).

[8] A. Celani and M. Vergassola, Phys. Rev. Lett. **108**, 258102 (2012).

[9] M. Skoge, Y. Meir, and N. S. Wingreen, Phys. Rev. Lett. **107**, 178101 (2011).

[10] Y. V Kalinin, L. Jiang, Y. Tu, and M. Wu, Biophys. J. **96**, 2439 (2009).

[11] R. Mesibov, G. W. Ordal, and J. Adler, J. Gen. Physiol. **62**, 203 (1973).

[12] T.-M. Yi, Y. Huang, M. I. Simon, and J. Doyle, Proc. Natl. Acad. Sci. **97**, 4649 (2000).

[13] G. L. Hazelbauer, J. J. Falke, and J. S. Parkinson, Trends Biochem. Sci. **33**, 9 (2008).

[14] G. Meacci, G. Lan, and Y. Tu, Biophys. J. **100**, 1986 (2011).

[15] M. Silverman and M. Simon, Nature **249**, 73 (1974).

[16] J. Saragosti, P. Silberzan, and A. Buguin, PLoS One **7**, e35412 (2012).

[17] L. Jiang, Q. Ouyang, and Y. Tu, PLoS Comput. Biol. **6**, e1000735 (2010).

[18] H. C. Berg, *E. Coli in Motion* (Springer, 2004).

[19] M. A. Rivero, R. T. Tranquillo, H. M. Buettner, and D. A. Lauffenburger, Chem. Eng. Sci. **44**, 2881 (1989).

[20] H. C. Berg, D. A. Brown, and others, Nature **239**, 500 (1972).

[21] S. P. Strong, B. Freedman, W. Bialek, and R. Koberle, Phys. Rev. E **57**, 4604 (1998).

[22] V. Sourjik and H. C. Berg, Proc. Natl. Acad. Sci. **99**, 123 (2002).

[23] M. K. Sarkar, K. Paul, and D. Blair, Proc. Natl. Acad. Sci. **107**, 9370 (2010).

[24] P. A. Spiro, J. S. Parkinson, and H. G. Othmer, Proc. Natl. Acad. Sci. **94**, 7263 (1997).

[25] H. C. Berg and L. Turner, Biophys. J. **58**, 919 (1990).

[26] Y. Tu, T. S. Shimizu, and H. C. Berg, Proc. Natl. Acad. Sci. **105**, 14855 (2008).

[27] N. Vladimirov, L. Løvdok, D. Lebiedz, and V. Sourjik, PLoS Comput. Biol. **4**, e1000242 (2008).

[28] M. Reneaux and M. Gopalakrishnan, J. Theor. Biol. **266**, 99 (2010).

[29] J. Taktikos, V. Zaburdaev, and H. Stark, Phys. Rev. E **85**, 51901 (2012).

[30] M. Flores, T. S. Shimizu, P. R. ten Wolde, and F. Tostevin, Phys. Rev. Lett. **109**, 148101 (2012).

[31] J. S. Parkinson, J. Bacteriol. **185**, 1492 (2003).

[32] T. S. Shimizu, Y. Tu, and H. C. Berg, Mol. Syst. Biol. **6**, (2010).